*fractal and fractional*

*Article*

# On Ikeda-Based Memristor Map with Commensurate and Incommensurate Fractional Orders: Bifurcation, Chaos, and Entropy

**Omar Alsayyed [1], Abderrahmane Abbes [2,*], Gharib Mousa Gharib [3], Mayada Abualhomos [4], Hassan Al-Tarawneh [5], Maha S. Al Soudi [6], Nabeela Abu-Alkishik [7], Abdallah Al-Husban [8] and Adel Ouannas [9]**

1 Department of Mathematics, Faculty of Science, The Hashemite University, P.O. Box 330127, Zarqa 13133, Jordan; omarm_re@hu.edu.jo
2 Laboratory of Mathematics, Dynamics and Modelization, Badji Mokhtar-Annaba University, Annaba 23000, Algeria
3 Department of Mathematics, Faculty of Science, Zarqa University, Zarqa 13110, Jordan; ggharib@zu.edu.jo
4 Applied Science Research Center (ASRC) , Applied Science Private University, Amman 11942, Jordan; abuhomos@asu.edu.jo
5 Department of Data Sciences and Artificial Intelligence, Al-Ahliyya Amman University, Amman 11942, Jordan; h.altarawneh@ammanu.edu.jo
6 Department of Basic Scientific Sciences, Applied Science Private University, Amman 11931, Jordan; m_alsoudi@asu.edu.jo
7 Department of Mathematics, Jerash University, Jerash 26150, Jordan; nabeelakishik@yahoo.com
8 Department of Mathematics, Faculty of Science and Technology, Irbid National University, P.O. Box 2600, Irbid 21110, Jordan; dralhosban@inu.edu.jo
9 Department of Mathematics and Computer Science, University of Larbi Ben M'hidi, Oum El Bouaghi 04000, Algeria; ouannas.adel@univ-oeb.dz
* Correspondence: abderrahmane.abbes@univ-annaba.dz

check for updates

**Citation:** Alsayyed, O.; Abbes, A.; Gharib, G.M.; Abualhomos, M.; Al-Tarawneh, H.; Al Soudi, M.S.; Abu-Alkishik, N.; Al-Husban, A.; Ouannas, A. On Ikeda-Based Memristor Map with Commensurate and Incommensurate Fractional Orders: Bifurcation, Chaos, and Entropy. *Fractal Fract.* **2023**, 7, 728. https://doi.org/10.3390/fractalfract7100728

Academic Editors: António Lopes, Faqiang Wang, Hongbo Cao and Shaobo He

Received: 7 August 2023
Revised: 9 September 2023
Accepted: 9 September 2023
Published: 1 October 2023



**Abstract:** This paper introduces a novel fractional Ikeda-based memristor map and investigates its non-linear dynamics under commensurate and incommensurate orders using various numerical techniques, including Lyapunov exponent analysis, phase portraits, and bifurcation diagrams. The results reveal diverse and complex system behaviors arising from the interplay of different fractional orders in the proposed map. Furthermore, the study employs the sample entropy test to quantify complexity and validate the presence of chaos. Non-linear controllers are also presented to stabilize and synchronize the model. The research emphasizes the system's sensitivity to the fractional order parameters, leading to distinct dynamic patterns and stability regimes. The memristor-based chaotic map exhibits rich and intricate behavior, making it an interesting and important area of research.

**Keywords:** Ikeda-based memristor map; discrete fractional calculus; bifurcation; chaotic dynamics; sample entropy; control

## 1. Introduction

Chaos theory has been extensively studied across various academic and engineering disciplines over the last few decades. This field of research has led to numerous interdisciplinary advancements with impressive performance in different domains [1–4]. The presence of randomness and unpredictability in chaotic systems and the sensitivity to initial conditions allow for the generation of pseudo-random sequences and enhanced data encryption. These inherent merits of chaotic behaviors have contributed to significant progress in various fields, including secure communications, image and signal processing, data encryption, and optimization algorithms, among others [5–8]. The rich dynamics of chaotic systems continue to inspire novel research and applications, making chaos theory an essential area of study with broad interdisciplinary impact.

A memory resistor, commonly known as a "memristor", has been widely recognized as a fourth fundamental circuit element that serves as a link between charge and magnetic flux. The theoretical concept of the memristor was initially forwarded by Chua in 1971 [9]. For an extended period, memristor research remained primarily theoretical until the first physical implementation of a memristor was achieved by HP laboratories in 2008. They successfully developed the first practical memristor using nanomaterials [10]. It has since become an essential component in various applications due to its unique properties and potential to revolutionize memory and computing technologies. Memristors have garnered significant attention and research interest, contributing to the advancement of various fields, including electronics [11], computing [12], nonvolatile memory [13], and neuromorphic systems [14].

In general, memristor-based chaotic systems are commonly designed using differential equations in the continuous-time domain [15]. However, until recent years, discrete-time memristive maps had not been extensively explored or discussed. In practice, discrete chaotic systems offer the advantage of avoiding parameter sensitivity issues present in continuous systems, making them easier to implement using digital hardware circuits [16]. Consequently, there has been a growing realization among researchers about the significance of exploring and understanding discrete memristive maps, leading to promising advancements in understanding the behavior of discrete memristor-based systems and their implications for various applications. Rong et al. [17] discussed the hidden Neimark–Sacker bifurcations of a three-dimensional Hénon map coupled by a memristor. The dynamics of a new memristive neuron map were presented in [18]. Almatroud and Pham [19] introduced a novel approach to construct free fixed-point maps by combining a cosine term with a memristor, and they investigated the dynamics of these proposed maps. The analysis of extremely hidden multistability and synchronization of memristor-coupled non-autonomous Fitzhugh–Nagumo models is shown in [20], whereas the hidden extreme multi-stability of a new 2D cosine memristor-based map is presented in [21]. These studies contribute to exploring the interactions between memristive elements and mathematical functions, providing valuable insights into the dynamics of memristive maps and their potential applications in various fields.

Discrete fractional calculus has emerged as a captivating research area that has grabbed the interest of mathematicians and scholars in various disciplines over the last decade. Its applications span diverse fields, including biology, ecology, and applied sciences, offering valuable insights into real-world challenges. Fractional systems have demonstrated the ability to describe complex nonlinear phenomena with greater accuracy compared to traditional integer-order systems [22], showcasing their unique properties, including long-term memory, viscosity, and flexibility. Recently, there has been a surge in published articles addressing this intriguing topic. Researchers have been offering various discrete-time fractional operators, conducting stability analyses, and presenting numerous theoretical findings [23–27]. Notably, Wu and Baleanu presented the first study that delves into the modeling of fractional chaotic maps using the left Caputo-like operator and investigated their chaotic characteristics [28]. As a result of these advances, this work has paved the way for the emergence of more commensurate- and non-commensurate-order chaotic maps [29–32], in addition to exploring diverse control strategies and synchronization schemes that have been developed to synchronize the interactions between different fractional discrete chaotic systems [33–35]. These studies reflected that the system's behavior is highly dependent on the chosen fractional order, showcasing its non-linear and complex nature, which makes it a fascinating subject of study in the field of fractional dynamics.

Indeed, the majority of the previous discrete memristors research has been focused on integer-order systems. Regrettably, the study of discrete fractional memristors remains inadequate, with relatively few studies dedicated to exploring their behavior and characteristics. For instance, Peng et al. investigated the chaotic behaviors in the Caputo fractional memristive map [36]. In [37], Lu et al. developed an innovative 2D discrete memristor map by incorporating a memristor into a 1D Rulkov neuron map, whereas in [38], the authors conducted an investigation into the multistability and synchronization of fractional maps resulting from the coupling of Rulkov neurons with locally active discrete memristors. Furthermore, the study of the frac memristor-based discrete chaotic map based on the Grunwald–Letnikov operator and its implementation in digital circuits is presented in [39]. Additionally, Shatnawi et al. recently explored the hidden attractors and multistability in a fractional non-fixed point discrete memristor-based map [40]. The study highlights the intricate and rich behavior of the system, emphasizing the significance of fractional components in contributing to the complexity and versatility of memristor-based maps. The majority of the research mentioned above has predominantly focused on commensurate-order models in discrete memristor-based maps. However, there appears to be a noticeable gap in the literature concerning the effect of the incommensurate-order case on the dynamics of such maps. In fact, the incommensurate order is a particular case of a fractional-order system by whether the order of each equation has different values. Thus, it improves the freedom of the models. This indicates an underexplored area in the field of discrete memristors, particularly in the context of incommensurate fractional memristors. Understanding the behavior and properties of incommensurate fractional memristors could lead to valuable insights and potential applications in various domains such as neural circuits, electronics, neural networks, viscoelasticity, control theory, neural dynamics, and so on [41–43]. Therefore, further investigation and research in this area are essential to uncovering the unique characteristics and potential benefits of incommensurate fractional memristors.

Motivated by the preceding discourse, our objective in this paper is to delve into the exploration and analysis of the dynamic behaviors exhibited by the fractional-order Ikeda-based memristor map, encompassing both commensurate and incommensurate fractional values. We undertake a comprehensive exploration of the fundamental properties of this Ikeda-based memristor map through a combination of numerical and theoretical analyses. The structure of this article is outlined as follows: In Section 2, we present the mathematical model of the discrete memristor and introduce essential preliminary concepts related to discrete fractional calculus. Section 3 introduces the fractional discrete version of the Ikeda-based memristor map. In Section 4, we delve into an analysis of the dynamic characteristics of the fractional Ikeda-based memristor map, focusing on both commensurate and incommensurate scenarios. This exploration is facilitated through Lyapunov exponent analysis, bifurcation diagrams, and phase attractor visualization. Section 5 involves the utilization of the sample entropy test ($SampEn$) to quantitatively measure complexity and validate the presence of chaos within the map. In Section 6, we propose adaptive nonlinear controllers aimed at stabilizing and synchronizing the proposed fractional Ikeda-based memristor map. Finally, we conclude the paper by summarizing the most noteworthy findings obtained throughout the study.

## 2. Discrete Memristor Mathematical Model

The memristor is a two-terminal nonlinear device that displays a pinched hysteresis in response to the application of any periodic voltage or current stimulation. Diverse memristors with discrete memristance values have been suggested through the use of differential modeling theory [44]. As per the concept presented in reference [45], the discrete memristor can be defined by:

$$\begin{cases} v_r = M(q_r)i_r, \\ q_{r+1} = q_r + k\, i_r, \end{cases} \tag{1}$$

where $k$ is constant. $v_r$ represents the output voltage, $i_r$ the input current, and $q_r$ represents the internal state of the discrete memristor at step $r$. $M(q_r)$ denotes the value of the discrete memristance function, which is equal, in this study, to:

$$M(q_r) = q_r^2 - 1.$$

Thus, the mathematical model for the discrete memristor (1) is formulated by:

$$\begin{cases} v_r = (q_r^2 - 1)i_r, \\ q_{r+1} = q_r + k\, i_r. \end{cases} \tag{2}$$

According to [46], for $i_r = A \sin \omega r$, the discrete memristor model can produce a hysteresis loop, as seen in Figure 1.

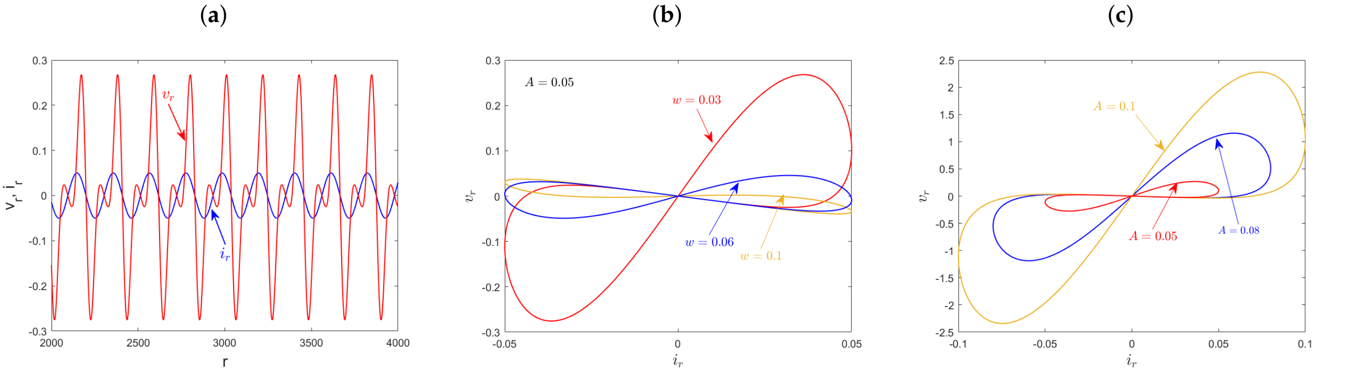


**Figure 1.** Discrete memristor characteristics (**a**) current and voltage for $q_0 = 0.1$, $A = 0.05$, $w = 0.03$; (**b**) pinched hysteresis loops for $w = 0.03, 0.06$ and $0.1$ and with fixed $q_0 = 0.1$, $A = 0.05$; (**c**) pinched hysteresis loops for $A = 0.05, 0.08$ and $0.1$ and with fixed $q_0 = 0.1$, $w = 0.03$.

The aforementioned equation, $q_{r+1} = q_r + ki_r$, allows for the expression of the correlation between the charge $q_r$ and current $i_r$, which is expressed as follows:

$$\begin{aligned} q_{r+1} &= q_r + k\, i_r \\ &= q_{r-1} + k\, i_{r-1} + k\, i_r \\ &= q_{r-2} + k\, i_{r-2} + k\, i_{r-1} + k\, i_r \\ &\;\;\vdots \\ &= q_0 + k\, i_0 + k\, i_1 + \cdots + k\, i_{r-2} + h\, i_{r-1} + k\, i_r. \end{aligned} \tag{3}$$

Thus:

$$q_r = q_0 + k \sum_{j=0}^{r-1} i_j. \tag{4}$$

Therefore, when we substitute Equation (4) into Equation (2), we obtain:

$$v_r = \left( \left( q_0 + k \sum_{j=0}^{r-1} i_j \right)^2 - 1 \right) i_r. \tag{5}$$

As demonstrated through Equation (5), the discrete memristor system exhibits "memory effects" resembling those of fractional discrete systems. This suggests that this memristor with integer-order characteristics has the potential to extend to fractional order. Hence, employing the Caputo operator yields the novel fractional discrete memristor system:

$$\begin{cases} v_r = (q_r^2 - 1)i_r, \\ {}^{C}\Delta_r^{\beta} q(v) = k\, i(v + \beta - 1), \end{cases} \tag{6}$$

where $v \in \mathbb{N}_{b-\beta+1}$ and $\beta \in (0, 1]$. The Caputo difference operator ${}^{C}\Delta_b^{\beta} Y(v)$ of a function $Y(v)$ is defined as follows:

**Definition 1** ([23]). *The β-th fractional sum for a function Y can be expressed as:*

$$\Delta_b^{-\beta} Y(v) = \frac{1}{\Gamma(\beta)} \sum_{l=b}^{b-\beta} (b-1-l)^{(\beta-1)} Y(l), \tag{7}$$

*with $v \in \mathbb{N}_{b+\beta}$, $\beta > 0$ and $\Gamma(.)$ is the Gamma function.*

**Definition 2** ([25]). *The Caputo-like difference operator for a function $Y(v)$ can be stated as:*

$$^{C}\Delta_v^{\beta} Y(b) = \Delta_b^{-(m-\beta)} \Delta^m X(v) = \frac{1}{\beta(m-\beta)} \sum_{l=b}^{v-(m-\beta)} (v-l-1)^{(m-\beta-1)} \Delta^m Y(l), \tag{8}$$

*where $v \in \mathbb{N}_{b+m-\beta}$, $\beta \notin \mathbb{N}$ and $m = \lceil \beta \rceil + 1$. $\Delta^m Y(v)$ and $(v-l-1)^{(m-\beta-1)}$ are the m-th integer difference operator and the falling factorial function, respectively, which are written as:*

$$\Delta^m Y(v) = \Delta(\Delta^{m-1} Y(v)) = \sum_{k=0}^{m} \binom{m}{k} (-1)^{m-k} Y(v+k), \qquad v \in \mathbb{N}_b, \tag{9}$$

*and*

$$(v-1-l)^{(m-\beta-1)} = \frac{\beta(v-l)}{\beta(v+1-l-m+\beta)}, \tag{10}$$

**Remark 1.** *For $m = 1$, we can define the Caputo-like operator by:*

$$^{C}\Delta_b^{\beta} Y(v) = \Delta_b^{-(1-\beta)} \Delta Y(v) = \frac{1}{\beta(1-\beta)} \sum_{l=b}^{v-(1-\beta)} (v-1-l)^{(-\beta)} \Delta Y(l), \quad v \in \mathbb{N}_{b-\beta+1} \tag{11}$$

Now, with the aid of the following theorem, we can figure out the numerical expression for the fractional discrete memristor system (6):

**Theorem 1** ([28]). *The solution of the following fractional difference system:*

$$\begin{cases} ^{C}\Delta_b^{\beta} Z(v) = Y(v+\beta-1, Z(v+\beta-1)) \\ \Delta^j Z(v) = Z_j, \quad m = \lceil \beta \rceil + 1, \end{cases} \tag{12}$$

*is expressed by:*

$$Z(v) = Z_0(v) + \frac{1}{\Gamma(\beta)} \sum_{l=m-\beta}^{v-\beta} (v+1-l)^{(\beta-1)} Y(l-1+\beta, Z(l-1+\beta)), \quad v \in \mathbb{N}_{b+m}, \tag{13}$$

*where:*

$$Z_0(v) = \sum_{j=0}^{m-1} \frac{(v-b)^j}{\Gamma(j+1)} \Delta^j Z(0). \tag{14}$$

The numerical representation of the fractional discrete memristor model (6) is designated according to the above theorem as follows:

$$\begin{cases} v_r = \left( \left( q_0 + \frac{k}{\Gamma(\beta)} \sum_{l=0}^{r-1} \frac{\Gamma(r-l-1+\beta)}{\Gamma(r-l)} i(l) \right)^2 - 1 \right) i_r, \\ q_r = q_0 + \frac{k}{\Gamma(\beta)} \sum_{l=0}^{r-1} \frac{\Gamma(r-l-1+\beta)}{\Gamma(r-l)} i(l). \end{cases} \tag{15}$$

By setting $q_0 = 0$ and utilizing the discrete current $i_r = A \sin(wr)$ as an input, with $w = 0.03$ representing the frequency and $A = 0.05$ denoting the amplitude, Figure 2 illustrates the characteristics of the input $i_r$ and output $v_r$ for different fractional orders. It is evident that the discrete memristor model displays hysteresis loops that converge at the origin, with the lobe region of the hysteresis loops progressively expanding as the fractional order value increases.

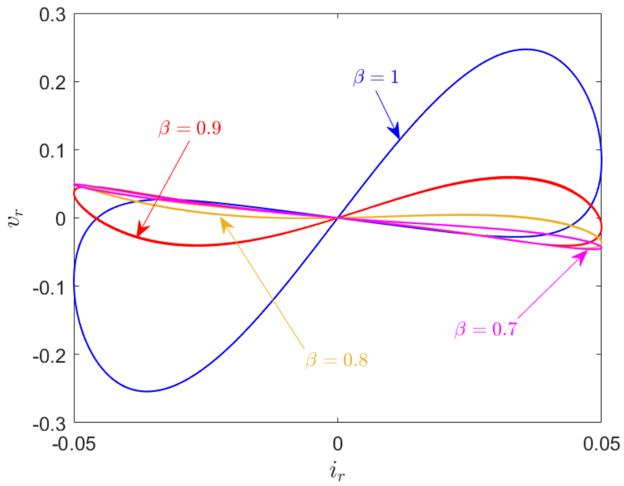


**Figure 2.** Pinched hysteresis loops of the discrete fractional memristor for $q(0) = 0.1$, $A = 0.05$, $w = 0.03$ and with different fractional order $\beta = 1, 0.9, 0.8$, and 0.7.

### 3. Fractional-Order Ikeda-Based Memristor Map

The original work of Ikeda [47] introduced the Ikeda map as a physical representation model to depict the behavior of light within a ring cavity, representing the propagation of light through a nonlinear optical resonator. Subsequently, in [48], the model was transformed into the following discrete-time system:

$$\begin{cases} y_1(r+1) = 1 + \rho(y_1(r)\cos\psi(r) - y_2(r)\sin\psi(r)), \\ y_2(r+1) = \rho(y_1(r)\sin\psi(r) + y_2(r)\cos\psi(r)), \end{cases} \tag{16}$$

where $\rho$ is bifurcation parameter and:

$$\psi(r) = 0.4 - \frac{0.6}{1 + y_1^2(r) + y_2^2(r)}$$

Laskaridis et al. [49] expanded the dimension of the Ikeda map by incorporating the discrete memristor model (2) into the map (16), yielding the following Ikeda-based memristor map:

$$\begin{cases} y_1(r+1) = 1 + \rho(y_1(r)\cos\psi(r) - y_2(r)\sin\psi(r)) + \mu(q^2(r) - 1)y_2(r), \\ y_2(r+1) = \rho(y_1(r)\sin\psi(r) + y_2(r)\cos\psi(r)), \\ q(r+1) = q(r) + y_2(r). \end{cases} \tag{17}$$

where $\mu$ is the controller parameter. Figure 3 presents the bifurcation diagram and Lyapunov exponents, as well as the phase attractor of the Ikeda-based memristor map, while varying $\rho$ from 0 to 0.7. The evidence presented in Figure 3 shows that the model demonstrates chaotic dynamics for a significant range of values, specifically within the interval $\rho \in (0.46, 0.53) \cup (0.61, 0.7)$.

In this investigation, we extend the integer-order Ikeda-based memristor map to generate the fractional-order Ikeda-based memristor map by employing the Caputo difference operator. The formula representing the first-order difference of the Ikeda-based memristor map is as follows:

$$\begin{cases} \Delta y_1(r) = 1 + \rho(y_1(r)\cos\psi(r) - y_2(r)\sin\psi(r)) + \mu(q^2(r) - 1)y_2(r) - y_1(r), \\ \Delta y_2(r) = \rho(y_1(r)\sin\psi(r) + y_2(r)\cos\psi(r)) - y_2(r), \\ \Delta q(r) = y_2(r), \end{cases} \tag{18}$$

where $\Delta y(r) = y(r+1) - y(r)$ is the standard difference operator. In the aforementioned system, if we substitute $\Delta$ with the Caputo-like operator ${}^C\Delta_b^\beta$ and replace $r$ with $\varrho = v + \beta - 1$, the resulting system becomes a fractional-order difference system.

$$\begin{cases} {}^C\Delta_b^\beta y_1(v) = 1 + \rho(y_1(\varrho)\cos\psi(\varrho) - y_2(\varrho)\sin\psi(\varrho)) + \mu(q^2(\varrho) - 1)y_2(\varrho) - y_1(\varrho), \\ {}^C\Delta_b^\beta y_2(v) = \rho(y_1(\varrho)\sin\psi(\varrho) + y_2(\varrho)\cos\psi(\varrho)) - y_2(\varrho), \\ {}^C\Delta_b^\beta q(v) = y_2(\varrho), \end{cases} \tag{19}$$

where $v \in \mathbb{N}_{b+1-\beta}$, $b$ is the initial point and $0 < \beta \le 1$ denotes the fractional order.

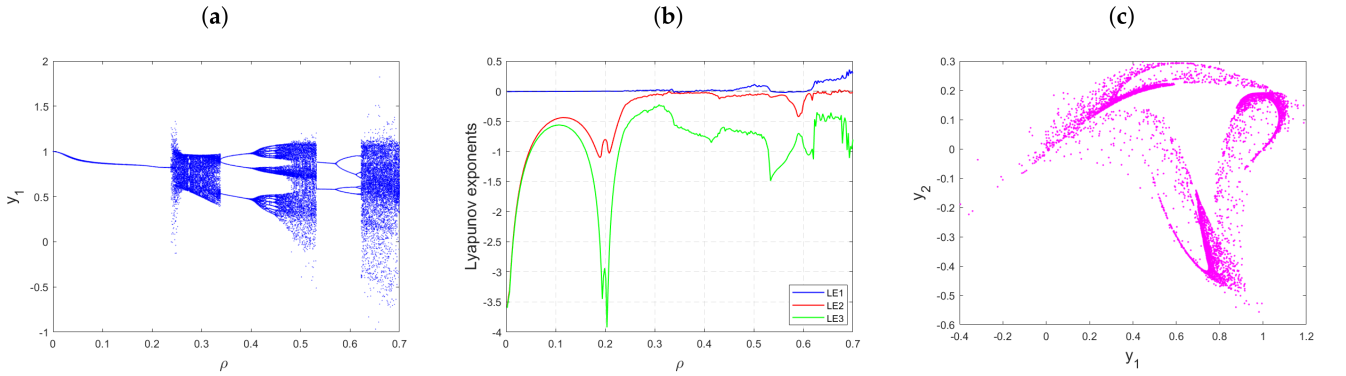

**Figure 3.** (**a**) Bifurcation diagram of (17) for $\rho$ ranging from 0 to 0.7. (**b**) The corresponding Lyapunov exponents. (**c**) Phase attractor of Ikeda-based memristor map.

## 4. Nonlinear Dynamics of the Fractional-Order Ikeda-Based Memristor Map

In this section, we will conduct an analysis of the behaviors of the fractional-order Ikeda-based memristor map (19). The analysis will be carried out across commensurate and incommensurate orders. We will employ a range of numerical tools, such as visualizing phase portraits, illustrating bifurcations, and estimating the maximum Lyapunov exponent ($LE_{max}$).

### *4.1. Commensurate-Order Fractional Ikeda-Based Memristor Map*

In this part, our focus is on elaborating on the different characteristics of the commensurate-order fractional Ikeda-based memristor map with the memristor. It is important to recognize that a commensurate-order fractional system comprises equations that possess identical orders. To this end, we will now supply the numerical formula, which will be presented in the following manner and is derived from Theorem 1:

$$\begin{cases} y_1(r) = y_1(0) + \sum\limits_{j=0}^{r-1} \frac{\Gamma(r-j-1+\beta)}{\Gamma(\beta)\Gamma(r-j)} \Big(1 + \rho(y_1(j)\cos\psi(j) - y_2(j)\sin\psi(j)) + \mu(q^2(j) - 1)y_2(j) - y_1(j)\Big), \\ y_2(r) = y_2(0) + \sum\limits_{j=0}^{r} \frac{\Gamma(r-j-1+\beta)}{\Gamma(\beta)\Gamma(r-j)} \Big(\rho(y_1(j)\sin\psi(j) + y_2(j)\cos\psi(j)) - y_2(j)\Big), \\ q(r) = q(0) + \sum\limits_{j=0}^{r} \frac{\Gamma(r-j-1+\beta)}{\Gamma(\beta)\Gamma(r-j)} \Big(y_2(j)\Big), \end{cases} \tag{20}$$

Setting $y_1(0) = y_2(0) = q(0) = 0.1$ and the parameter $\mu = 0.11$, we plot three bifurcations of (19) associated with $\rho \in [0,1]$, as shown in Figure 4, which correspond to the parameter $\mu = 0.11$ and the commensurate orders $\beta = 0.1$, $\beta = 0.3$, and $\beta = 0.9$. It is evident that both the parameter's system $\rho$ and the commensurate order $\beta$ have an effect on the states of the commensurate fractional Ikeda-based memristor map (19). Indeed, as the commensurate fractional order $\beta$ decreases and the parameter $\rho$ increases, the commensurate fractional Ikeda-based memristor map (19) displays a more extended chaotic region. This leads to the emergence of more complex oscillations and increased unpredictability in the system's behavior. The interplay between the fractional order and the system parameter has a significant impact on the dynamical behavior, and these changes can result in a richer range of chaotic patterns and intricate trajectories within the Ikeda-based memristor map (19).

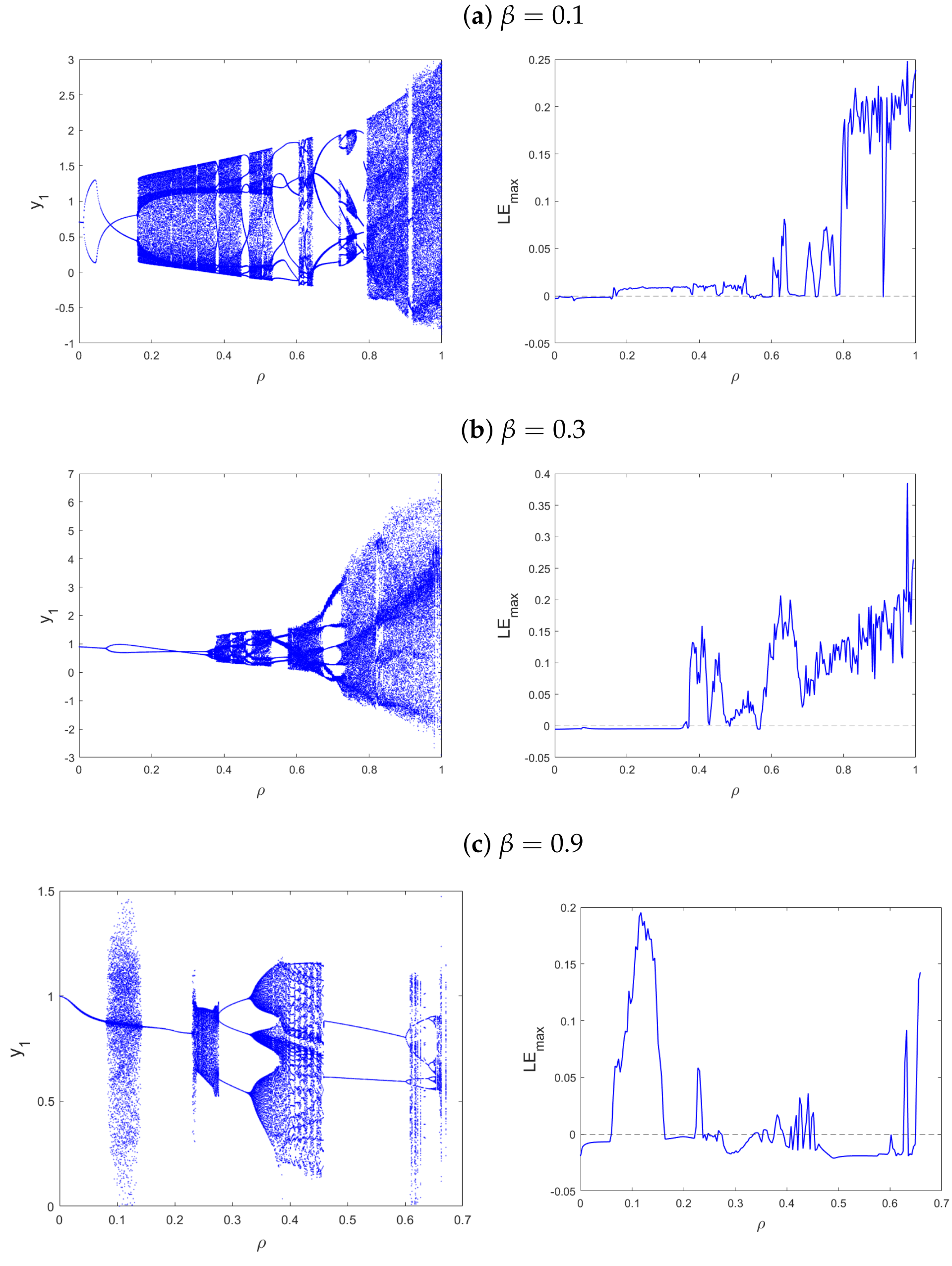


**Figure 4.** (**a**) Three Bifurcation diagrams of $y_1$ and their $LE_{max}$ associated with $\rho$, for (**a**) $\beta = 0.1$, (**b**) $\beta = 0.3$, and (**c**) $\beta = 0.9$.

Now, considering $\beta$ as the critical parameter, the bifurcation diagram is used to depict the variations in the behaviors of the commensurate Ikeda-based memristor map (19) as the order $\beta$ is varied from 0 to 1 with step size 0.001. Figure 5 depicts the bifurcation and the $LE_{max}$. We can see that upon changing the commensurate order, a rich set of dynamic characteristics (chaotic and regular) of the fractional map are investigated in regards to the commensurate order $\beta$. In more detail, there are regions where the system oscillates chaotically and regions where the system oscillates regularly. More specifically, when $\beta \in (0, 0.04)$, periodic windows with nine-period orbits appear, with the occurrence of a small chaotic motion in the interval $(0.04, 0.16)$. When $\beta \in (0.22, 0.31)$, we can observe oscillations between chaotic and regular trajectories in the states of the commensurate Ikeda-based memristor map (19). During this range, the $LE_{max}$ also fluctuates between positive and negative values, indicating transitions between chaotic and non-chaotic behaviors in the system. When the commensurate order $\beta$ falls within the range of $(0.31, 0.58)$, the trajectories of the commensurate-order Ikeda-based memristor map exhibit chaotic behavior. However, as $\beta$ transitions to the range of $(0.58, 0.95)$, two-period orbits emerge, indicating the stability of the model. Subsequently, for larger values of $\beta$, chaotic motions reappear, characterized by a positive maximum Lyapunov exponent ($LE_{max}$), indicating chaotic dynamics in the trajectories of the commensurate-order Ikeda-based memristor map. These described dynamic features are further confirmed by the $LE_{max}$ shown in Figure 5, providing additional evidence for the system's complex and diverse behavior and confirming the sensitivity of the map to changes in the commensurate-order parameter $\beta$. Furthermore, based on the observation of the maximum Lyapunov exponent, it can be concluded that when the $LE_{max}$ is not positive, the commensurate Ikeda-based memristor map exhibits regular oscillations. Conversely, the presence of chaotic oscillations is inferred when the exponent is positive. In order to achieve a comprehensive understanding of these characteristics, Figure 6 displays the discrete time evolution of the states $y_1$, $y_2$, and $q$ in the suggested commensurate map. Additionally, Figure 7 illustrates the phase portraits for various values of the commensurate order $\beta$ ($\beta = 0.1$, $\beta = 0.4$, $\beta = 0.6$, $\beta = 0.9$, $\beta = 0.98$, and $\beta = 1$). From the figures, the observed trajectories in the proposed commensurate map switch between chaotic oscillations and periodic behaviors as the commensurate order $\beta$ varies. This observation emphasizes the sensitivity of the system to changes in $\beta$ and demonstrates the richness and complexity of the dynamical properties in the commensurate-order Ikeda-based memristor map (19).

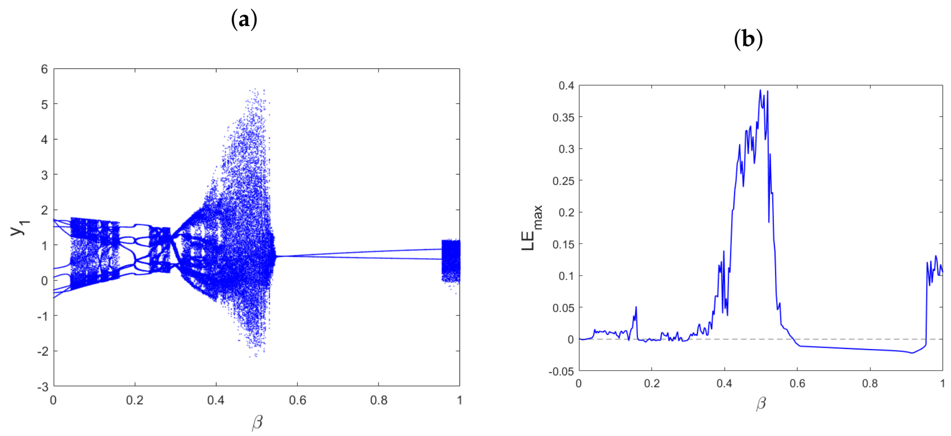


**Figure 5.** (**a**) Bifurcation of commensurate order Ikeda-based memristor map (19) for $\beta \in (0, 1)$. (**b**) The corresponding $LE_{max}$.

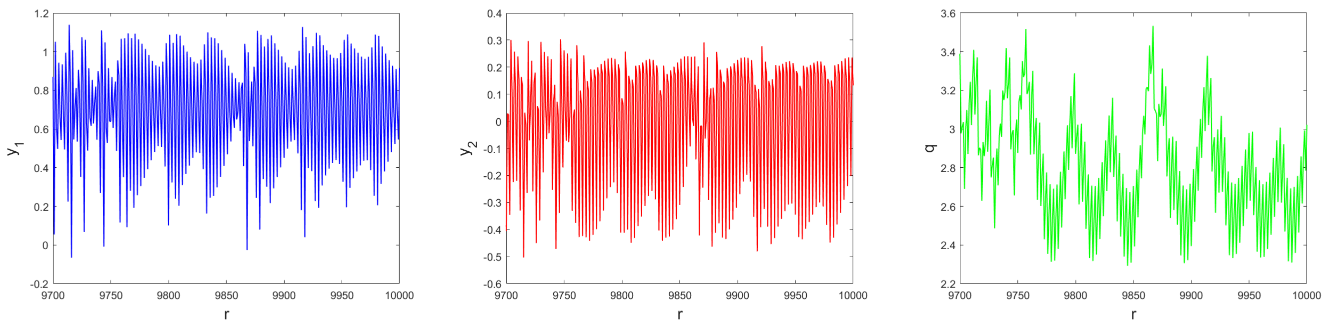


**Figure 6.** Time evolution of (19) for $\beta = 0.98$.

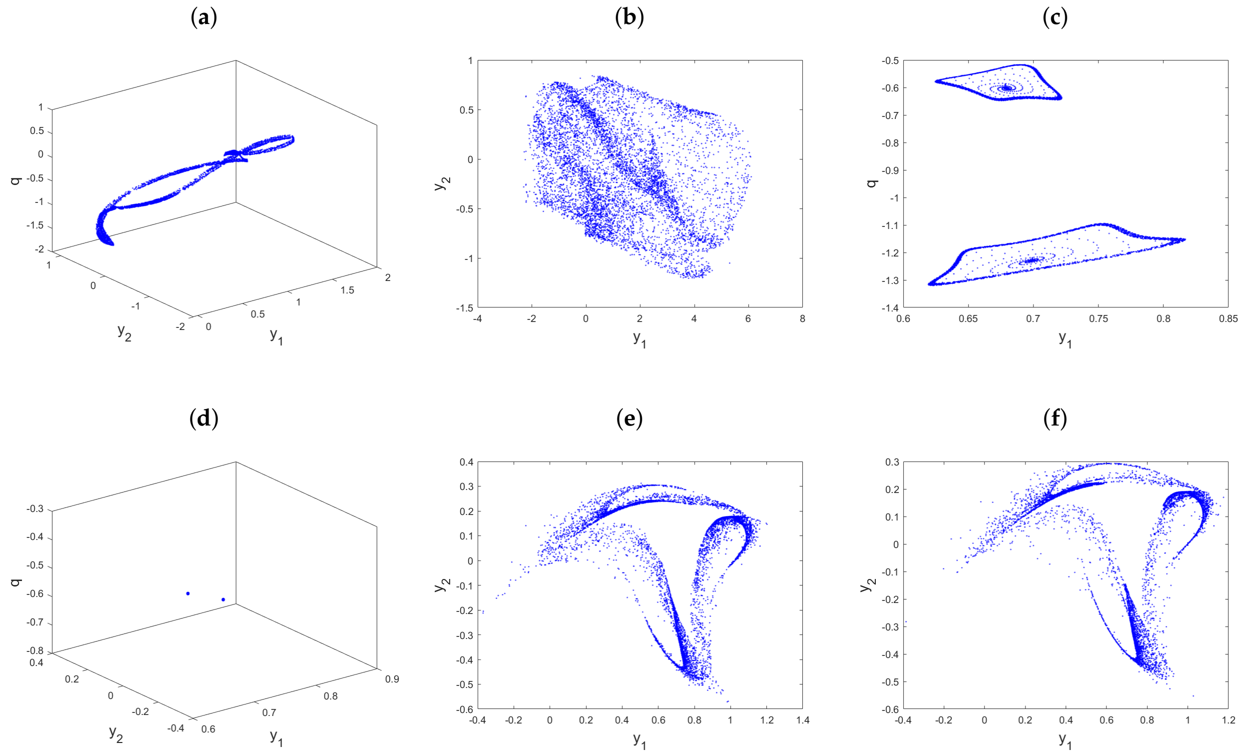

**Figure 7.** Phase portraits of (19) for different values of $\beta$ (**a**) $\beta = 0.1$, (**b**) $\beta = 0.4$, (**c**) $\beta = 0.6$, (**d**) $\beta = 0.9$, (**e**) $\beta = 0.98$, (**f**) $\beta = 1$.

### 4.2. Incommensurate-Order Fractional Ikeda-Based Memristor Map

In this section, we delve into the dynamics of the incommensurate-order fractional Ikeda-based memristor map. The concept of incommensurate order entails utilizing different fractional orders for each equation within the system. The representation of the incommensurate-order fractional Ikeda-based memristor map is as follows:

$$\begin{cases} {}^{c}\Delta_{b}^{\beta_1} y_1(v) = 1 + \rho(y_1(\varrho)\cos\psi(\varrho) - y_2(\varrho)\sin\psi(\varrho)) + \mu(q^2(\varrho) - 1)y_2(\varrho) - y_1(\varrho), \\ {}^{c}\Delta_{b}^{\beta_2} y_2(v) = \rho(y_1(\varrho)\sin\psi(\varrho) + y_2(\varrho)\cos\psi(\varrho)) - y_2(\varrho), \\ {}^{c}\Delta_{b}^{\beta_3} q(v) = y_2(\varrho), \end{cases} \tag{21}$$

By utilizing Theorem 1, we can express the numerical representation of the incommensurate fractional Ikeda-based memristor map (21) as follows:

$$\begin{cases} y_1(r) = y_1(0) + \sum\limits_{j=0}^{r-1} \frac{\Gamma(r-j-1+\beta_1)}{\Gamma(\beta_1)\Gamma(r-j)} \Big(1 + \rho(y_1(j)\cos\psi(j) - y_2(j)\sin\psi(j)) + \mu(q^2(j) - 1)y_2(j) - y_1(j)\Big), \\ y_2(r) = y_2(0) + \sum\limits_{j=0}^{r} \frac{\Gamma(r-j-1+\beta_2)}{\Gamma(\beta_2)\Gamma(r-j)} \Big(\rho(y_1(j)\sin\psi(j) + y_2(j)\cos\psi(j)) - y_2(j)\Big), \\ q(r) = q(0) + \sum\limits_{j=0}^{r} \frac{\Gamma(r-j-1+\beta_3)}{\Gamma(\beta_3)\Gamma(r-j)} \Big(y_2(j)\Big), \end{cases} \tag{22}$$

We analyze the dynamics and characteristics of this map to understand its unique behavior and explore the implications of employing distinct fractional orders in the system's equations. The three bifurcation diagrams presented in Figure 8 demonstrate the behaviors of the incommensurate Ikeda-based memristor map (21) as the parameter $\rho$ varies within the range $[0, 1]$. The simulations were conducted with the value of parameter $\mu = 0.11$ and initial conditions $(y_1(0), y_2(0), q(0))$=$(0.1, 0.1, 0.1)$. It is evident that these diagrams exhibit distinct patterns, indicating that the change in fractional orders $(\beta_1, \beta_2, \beta_3)$ significantly impacts the states of the incommensurate order fractional Ikeda-based memristor map (21). For instance, when $(\beta_1, \beta_2, \beta_3)$ = $(1, 0.1, 0.1)$, the system's states evolve from periodic to chaotic behavior with periodic doubling bifurcation as the parameter $\rho$ increases. On the other hand, when $(\beta_1, \beta_2, \beta_3) = (0.1, 0.5, 0.1)$, oscillatory motion is observed, with trajectories remaining stable for small values of $\rho$ and becoming chaotic as $\rho$ approaches 1. In the case of $(\beta_1, \beta_2, \beta_3) = (0.1, 0.1, 0.7)$, a chaotic region is evident throughout the interval, except for some small regions where the model exhibits regular oscillations, especially when $\rho$ approaches 0. To provide a more detailed illustration of the influence of incommensurate orders on the behaviors of the Ikeda-based memristor map, further investigation has been carried out in three specific cases. These investigations offer a deeper understanding of how the fractional orders impact the system dynamics and underscore the importance of considering incommensurate orders in the analysis of the model's behavior.

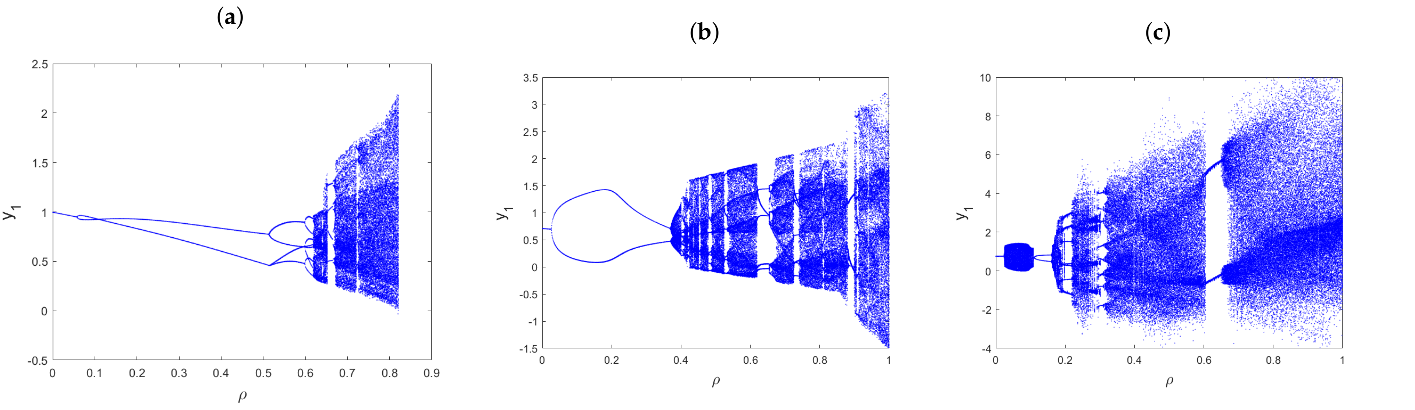


**Figure 8.** Bifurcations of (21) versus the parameter system $\rho$ for (**a**) $(\beta_1, \beta_2, \beta_3) = (1, 0.1, 0.1)$, (**b**) $(\beta_1, \beta_2, \beta_3) = (0.1, 0.5, 0.1)$, (**c**) $(\beta_1, \beta_2, \beta_3) = (0.1, 0.1, 0.7)$.

Case 1. In Figure 9a,b, we observe the variation of the order $\beta_1$ from 0 to 1 with a step size of $\Delta\beta_1 = 0.001$. These figures illustrate the bifurcation and its corresponding Lyapunov exponent of the incommensurate-order fractional Ikeda-based memristor map (21) for $\beta_2 = \beta_3 = 0.1$, the parameter value $\rho = 0.5$, $\mu = 0.11$, and the initial conditions $(y_1(0), y_2(0), q(0))$=$(0.1, 0.1, 0.1)$. From Figure 9a, it is evident that the state of the incommensurate Ikeda-based memristor map (21) exhibits chaotic behavior for smaller values of $\beta_1$, as evidenced by positive $LE_{max}$, as shown in Figure 9b. The Lyapunov exponent ($LE_{max}$) displayed in Figure 9b fluctuates between positive and negative values when $\beta_1$ lies within the region (0.24, 0.36). This outcome indicates the presence of chaotic behavior with the emergence of periodic windows. As the incommensurate order $\beta_1$ increases further, the trajectories transition from chaotic to regular motion, characterized by two-period orbits where the states of the incommensurate order fractional Ikeda-based memristor map (21) become stable.

Case 2. The bifurcation diagram and its ($LE_{max}$) are plotted to investigate the dynamic behaviors of the incommensurate order fractional Ikeda-based memristor map (21), with $\beta_2$ being an adjustable parameter, as depicted in Figure 10. The simulations are conducted by varying $\beta_2$ in the range $(0, 1]$, while keeping the incommensurate orders $\beta_1 = \beta_3 = 0.1$, initial conditions $(y_1(0), y_2(0), q(0)) = (0.1, 0.1, 0.1)$, and parameter values unchanged. From the figure, it can be observed that as the order $\beta_2$ increases to larger values, the trajectories become more stable. On the other hand, as $\beta_2$ decreases, chaotic behaviors emerge with positive values of $LE_{max}$, along with the appearance of small periodic regions exhibiting negative values of $LE_{max}$. Additionally, as $\beta_2$ decreases even further and approaches 0, the maximum Lyapunov exponent values decrease until they reach zero. This indicates that periodic trajectories appear and signifies that the incommensurate fractional Ikeda-based memristor map (21) undergoes a transition from chaotic to regular behavior. The observed changes in the $LE_{max}$ and the corresponding dynamic patterns illustrate the system's sensitivity to variations in the parameter $\beta_2$, highlighting the complexity and versatility of the incommensurate-order fractional Ikeda-based memristor map.

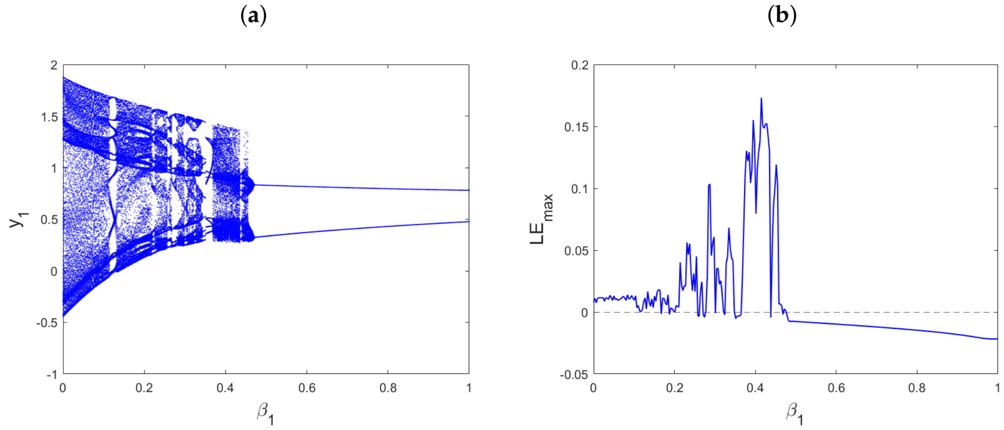


**Figure 9.** (**a**) Bifurcation of (21). (**b**) Corresponding $LE_{max}$ versus the incommensurate fractional order $\beta_1$ for $\beta_2 = \beta_3 = 0.1$.

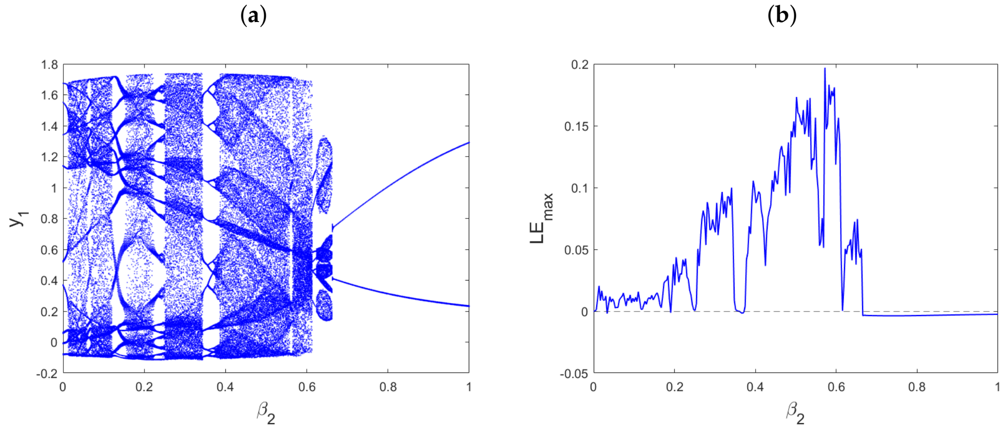


**Figure 10.** (**a**) Bifurcation of (21). (**b**) Corresponding $LE_{max}$ versus the incommensurate fractional order $\beta_2$ for $\beta_1 = \beta_3 = 0.1$.

Case 3. The bifurcation chart and its corresponding $LE_{max}$ of the proposed new incommensurate-order fractional Ikeda-based memristor map (21) are presented in Figure 11, where the parameter $\beta_3$ is varied within the range $(0, 1)$. In this analysis, we maintain the incommensurate orders as $\beta_1 = \beta_2 = 0.1$. From Figure 11, it is evident that unlike the previous cases, the trajectories of the incommensurate model exhibit chaotic behavior when the order $\beta_3$ takes larger values, as indicated by the higher values of $LE_{max}$. We see also see that when $\beta_3$ approaches 1, the map shows transition states and the trajectories go to infinity, for example, when $\beta_3 = 0.9$ and after some number of iterations, especially $r = 4997$, the trajectories diverge toward infinity, as presented in Figure 12. As $\beta_3$ continues to decrease, the $LE_{max}$ starts decreasing as well, reaching its smallest value, leading to a reduction in chaos and, consequently, the behavior of the map's states becomes more stable. These results emphasize the sensitivity of the incommensurate fractional Ikeda-based memristor map (21) to changes in the order $\beta_3$, resulting in a diverse range of dynamic behaviors, including chaotic and periodic motion. This highlights the significance of incommensurate orders in shaping the system's dynamics. Additionally, the phase portraits of the state variables of the incommensurate fractional Ikeda-based memristor map (21), as shown in Figure 13, further support the notion that incommensurate orders more accurately represent the system's behaviors. Overall, the study emphasizes the intricate and diverse nature of the incommensurate-order fractional Ikeda-based memristor map and the significance of the choice of fractional orders in modeling and characterizing its dynamics.

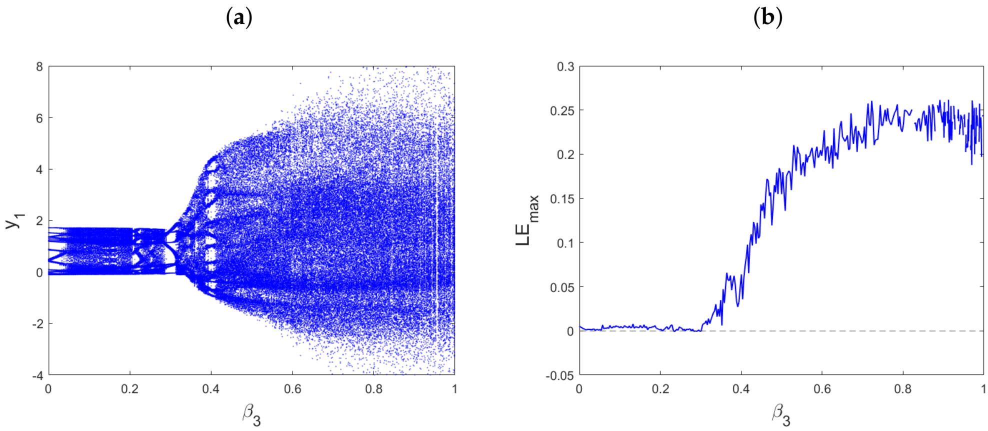


**Figure 11.** (**a**) Bifurcation of (21). (**b**) Corresponding $LE_{max}$ versus the incommensurate fractional order $\beta_3$ for $\beta_1 = \beta_2 = 0.1$.

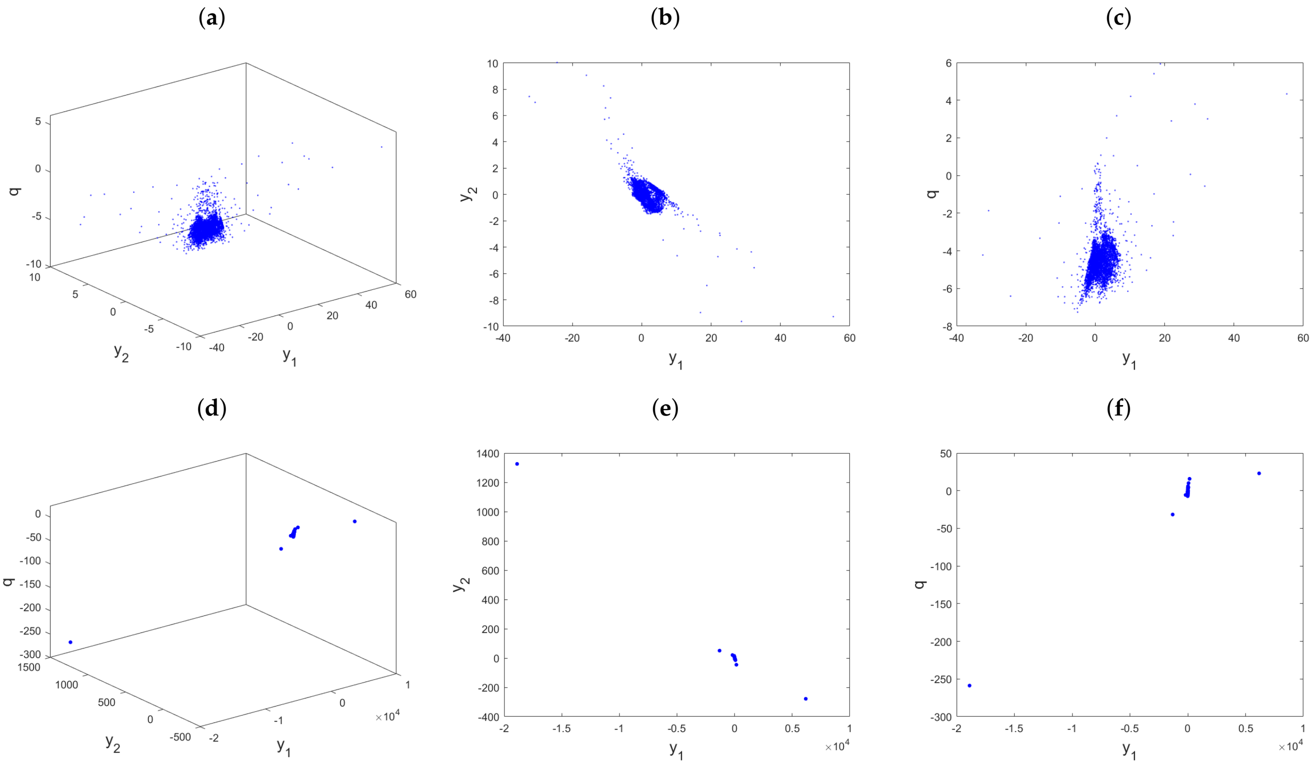


**Figure 12.** Phase portraits of (21) for $(\beta_1, \beta_2, \beta_3) = (0.1, 0.1, 0.7)$ and (**a**) $r = 4990$, (**b**) $r = 4997$.

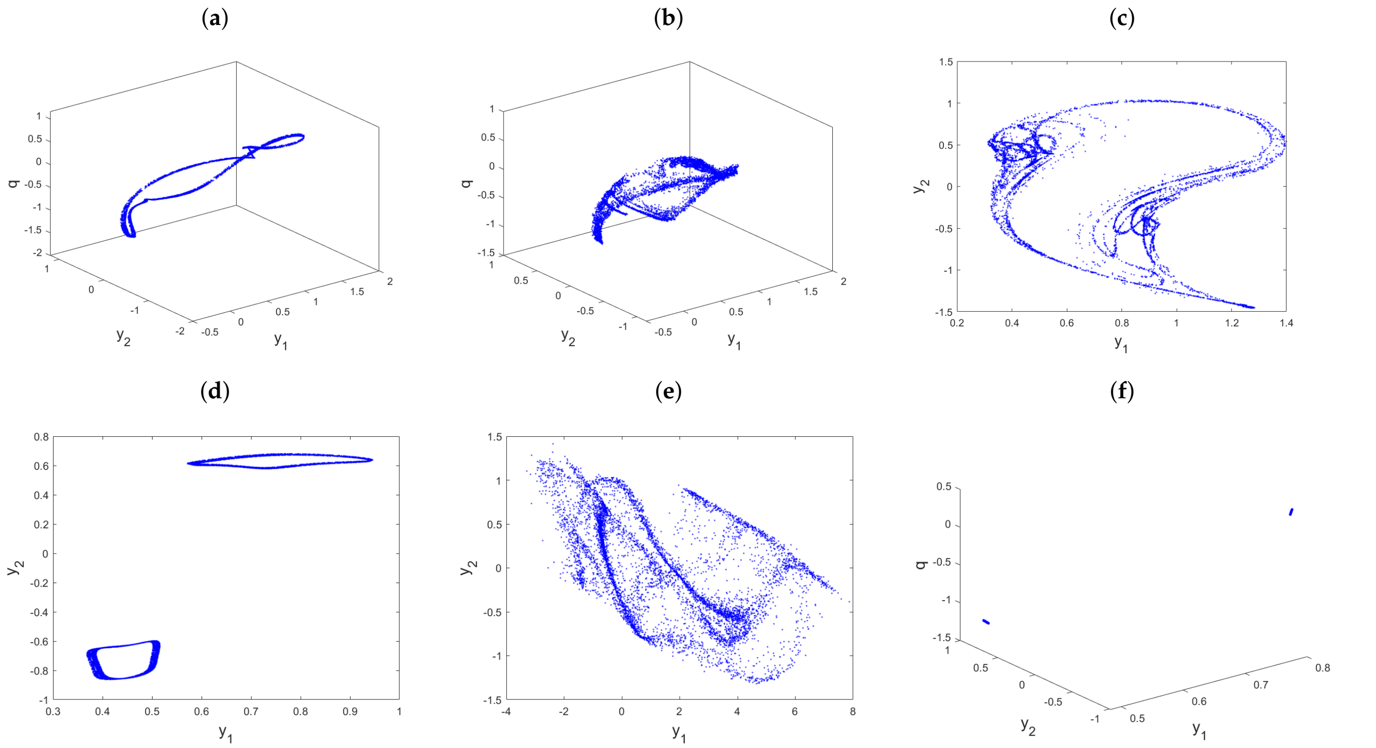


**Figure 13.** Phase portraits of (21) for different values of incommensurate orders $\beta_1$, $\beta_2$, and $\beta_3$; **(a)** $(\beta_1, \beta_2, \beta_3) = (0.1, 0.1, 0.05)$, **(b)** $(\beta_1, \beta_2, \beta_3) = (0.1, 0.5, 0.1)$, **(c)** $(\beta_1, \beta_2, \beta_3) = (0.4, 0.1, 0.1)$, **(d)** $(\beta_1, \beta_2, \beta_3) = (0.1, 0.65, 0.1)$, **(e)** $(\beta_1, \beta_2, \beta_3) = (0.1, 0.1, 0.7)$, **(f)** $(\beta_1, \beta_2, \beta_3) = (1, 0.1, 0.1)$.

## 5. The Sample Entropy Test (*SampEn*)

In this study, we employ the sample entropy (SampEn) method to assess the complexity of both the commensurate-order fractional Ikeda-based memristor map (19) and the incommensurate-order fractional Ikeda-based memristor map (21). Unlike approximate entropy (ApEn), SampEn can effectively measure the irregularity of time series regardless of the embedding dimension ($j$) and the similarity coefficient ($t$). Consequently, SampEn provides a more consistent and unbiased measure compared to ApEn [50]. The SampEn values indicate the complexity level of the time series, with higher values corresponding to higher complexity [51]. The calculation of SampEn is performed as follows:

We first define $r - j + 1$ vectors as follows:

$$Y(i) = [y_1(i), ..., y_1(i + m - 1)], \tag{23}$$

for $i \in [1, r - j + 1]$, where $y_1(1), y_1(2), ..., y_1(n)$ is a set of discrete points. In addition, we describe the following equation:

$$C_i^j(t) = \frac{K}{r - j + 1}, \tag{24}$$

where $K$ is the number of $Y(i)$ having $d(Y(i), Y(l)) \leq t$. Here, we set $j = 2$ and $t = 0.2std(Y)$, where $std(Y)$ is the standard deviation of the data $Y$. Theoretically, the ApEn is calculated as:

$$SampEn = -\log \frac{\Psi^{j+1}(r)}{\Psi^j(r)}, \tag{25}$$

where $\Psi^j(t)$ is expressed as:

$$\Psi^j(t) = \frac{1}{r - j + 1} \sum_{i=1}^{r-j+1} \log C_i^j(t). \tag{26}$$

The sample entropy results for the commensurate-order fractional Ikeda-based memristor map (19) and the incommensurate-order fractional Ikeda-based memristor map (21) are presented in Figure 14, with initial conditions set as $(y_1(0), y_2(0), q(0)) = (0.1, 0.1.0, 1)$. The obtained $SampEn$ values indicate the complexity levels of the time series, with larger values corresponding to higher complexity. The results demonstrate that both the commensurate and incommensurate fractional Ikeda-based memristor maps exhibit higher complexity, as indicated by their larger $SampEn$ values. These findings align with the results obtained from the maximum Lyapunov exponent analysis, further confirming the chaotic nature of the dynamics in the proposed fractional system. The higher complexity and chaotic behavior support the significance of fractional orders in capturing the rich dynamics of the proposed fractional Ikeda-based memristor map.

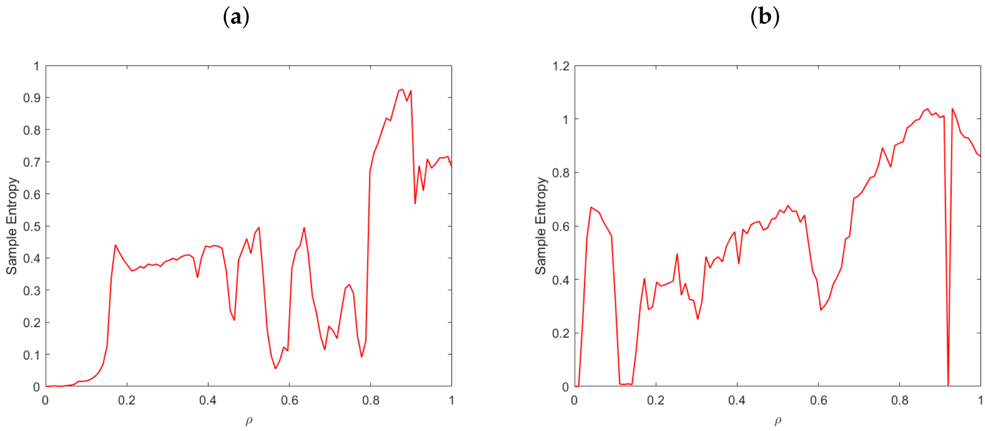


**Figure 14.** The sample entropy results of the fractional Ikeda-based memristor map versus the parameter $\rho$ for (**a**) $\beta = 0.1$, (**b**) $(\beta_1, \beta_2, \beta_3) = (0.1, 0.1, 0.7)$.

On the other hand, to get a better understanding of the influence of the fractional order on the Ikeda-based memristor map and in light of previous numerical findings, we compare the sample entropy results obtained from the fractional Ikeda-based memristor map with the results obtained from the fractional-order Ikeda map, which are presented in Table 1. One can observe that the fractional-order Ikeda-based memristor map generates a chaotic sequence with a greater degree of complexity than that of the classical fractional Ikeda-based memristor map. Consequently, we can conclude that the sample entropy test is an effective tool for measuring the complexity of the proposed map accurately.

**Table 1.** The sample entropy test.

| $\beta_1$ | 0.1 | 0.1 | 0.4 | 0.4 | 1 | 0.8 | 1 |
|---|---|---|---|---|---|---|---|
| $\beta_2$ | 0.1 | 0.5 | 0.1 | 0.4 | 0.1 | 0.8 | 1 |
| $\beta_3$ | 0.1 | 0.1 | 0.1 | 0.4 | 0.1 | 0.8 | 1 |
| $SampEn$ of Ikeda memristor map | 0.4363 | 0.5188 | 0.7081 | 0.8150 | 0.0468 | 0.0029 | 0.4542 |
| $SampEn$ of Ikeda map | 0.4066 | 0.1596 | 0.5909 | 0.4899 | 0.0602 | 0.0046 | 0 |

## 6. Control of Fractional Ikeda-Based Memristor Map

### *6.1. Stabilisation of Fractional Ikeda-Based Memristor Map*

Here, a stabilization controller is proposed to stabilize the suggested fractional Ikeda-based memristor chaotic map. The main objective of the stabilization method is to design an effective adaptive controller that drives all states of the map towards zero asymptotically. To achieve this goal, we begin by revisiting the stability theorem for the fractional maps.

**Theorem 2** ([52])**.** *Let $y(r) = (y_1(r), \ldots, y_n(r))^T$ and $B \in \mathcal{M}_n(\mathbb{R})$. The zero equilibrium point of the linear fractional-order discrete system:*

$$^{C}\Delta_b^{\beta} y(r) = B\, y(\varrho), \tag{27}$$

*$\forall\, r \in \mathbb{N}_{b+1-\beta}$ is asymptotically stable if:*

$$\lambda_\iota \in \left\{ \gamma \in \mathbb{C} : |\gamma| < \left( 2\cos\frac{|\arg\gamma| - \pi}{2-\beta} \right)^{\beta} \quad \text{and} \quad |\arg\gamma| > \frac{\beta\,\pi}{2} \right\}, \tag{28}$$

*where $\lambda_\iota$ are the eigenvalues of the matrix $B$.*

Now, the controlled fractional Ikeda-based memristor map is given by:

$$\begin{cases} ^{c}\Delta_b^{\beta} y_1(v) = 1 + \rho(y_1(\varrho)\cos\psi(\varrho) - y_2(\varrho)\sin\psi(\varrho)) + \mu(q^2(\varrho) - 1)y_2(\varrho) - y_1(\varrho) + C_1(\varrho), \\ ^{c}\Delta_b^{\beta} y_2(v) = \rho(y_1(\varrho)\sin\psi(\varrho) + y_2(\varrho)\cos\psi(\varrho)) - y_2(\varrho) + C_2(\varrho), \\ ^{c}\Delta_b^{\beta} q(v) = y_2(\varrho) + C_3(\varrho), \end{cases} \tag{29}$$

where $\varrho = v + \beta - 1$ and $C = (C_1, C_2, C_3)^T$ is the adaptive controller. The following theorem introduces control laws aimed at stabilizing the proposed novel fractional Ikeda-based memristor map.

**Theorem 3.** *If suitable control laws are designed as follows:*

$$\begin{cases} C_1(\varrho) = -1 - \rho(y_1(\varrho)\cos\psi(\varrho) - y_2(\varrho)\sin\psi(\varrho)) - \mu(q^2(\varrho) - 1)y_2(\varrho), \\ C_2(\varrho) = -\rho(y_1(\varrho)\sin\psi(\varrho) + y_2(\varrho)\cos\psi(\varrho)), \\ C_3(\varrho) = -y_2(\varrho) - q(\varrho). \end{cases} \tag{30}$$

*Then, the fractional Ikeda-based memristor map can be stabilized at its equilibrium point.*

**Proof.** Substituting $C_1$, $C_2$, and $C_3$ into (29) yields the following linear system:

$$^{C}\Delta_b^{\beta} Y(r) = BY(\varrho), \tag{31}$$

where $Y = (y_1, y_2, q)^T$ and:

$$B = \begin{pmatrix} -1 & 0 & 0 \\ 0 & -1 & 0 \\ 0 & 0 & -1 \end{pmatrix}$$

It is easy to see that the eigenvalues of the matrix $B$ satisfy:

$$|\lambda_j| = 1 < \left( 2\cos\frac{|\arg\lambda_j| - \pi}{2-\beta} \right)^{\beta} \quad \text{and} \quad |\arg\lambda_j| = \pi > \frac{\beta\,\pi}{2}, \quad j = 1, 2, 3.$$

So, by employing Theorem 2, the controlled fractional Ikeda-based memristor map is asymptotically stable. □

To validate the findings of Theorem 3, numerical simulations were performed. Figures 15 and 16 present the time series of the controlled fractional Ikeda-based memristor map (29). It is evident from the figure that the system's states approach zero asymptotically, confirming the successful stabilization results.

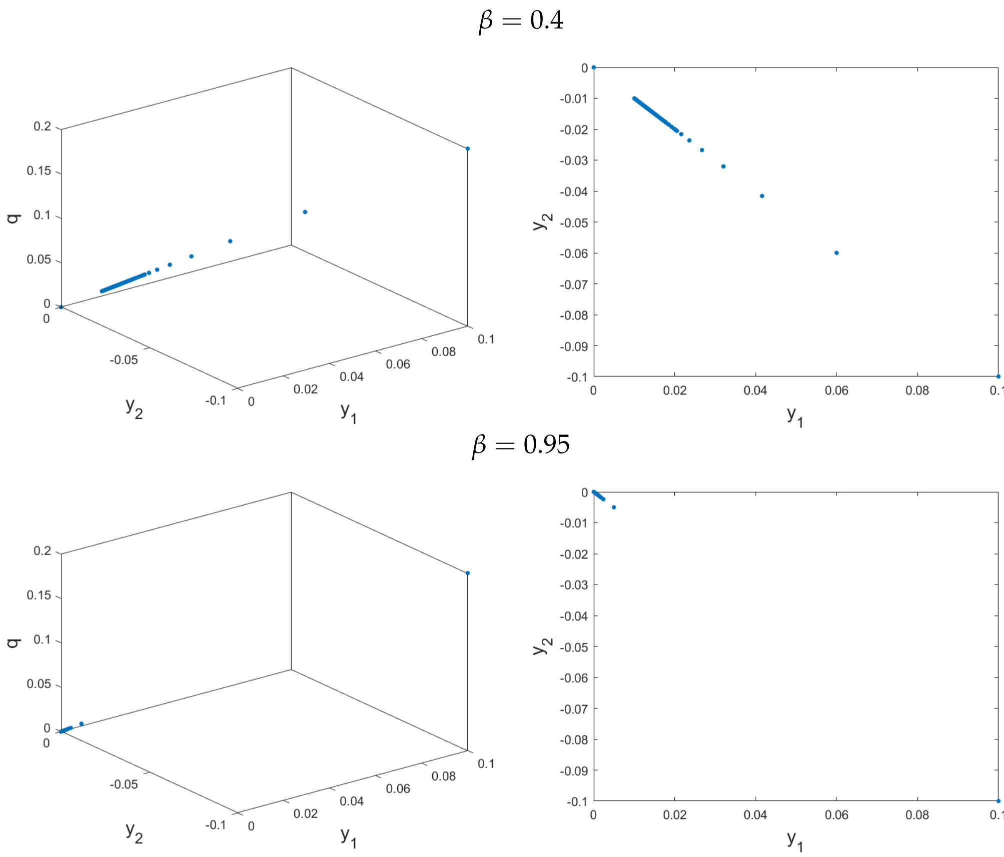


**Figure 15.** Attractors of the controlled fractional Ikeda-based memristor map (29) for $\beta = 0.4, 0.95$ and initial condition $(y_1(0), y_2(0), q(0)$=$(0.1, -0.1, 0.2)$.

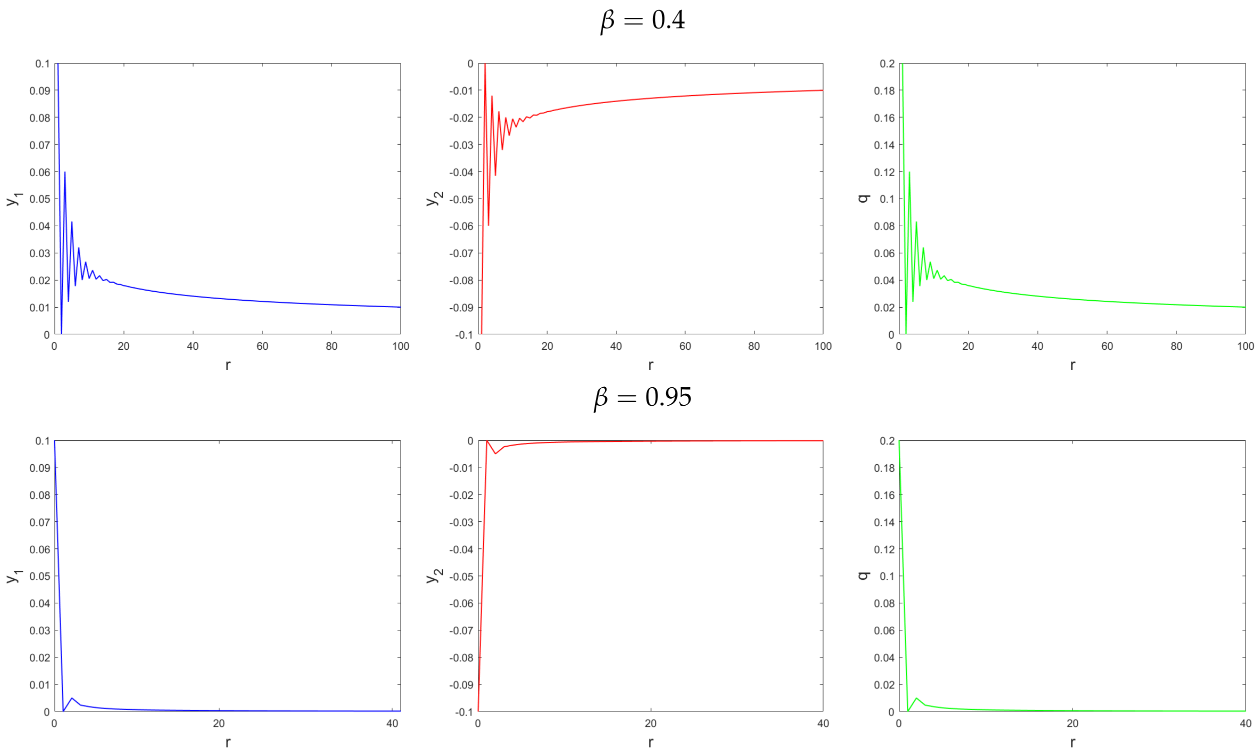


**Figure 16.** The stabilized states of the controlled fractional Ikeda-based memristor map (29) for $\beta = 0.4, 0.95$ and initial condition $(y_1(0), y_2(0), q(0)$=$(0.1, -0.1, 0.2)$.

*6.2. Synchronization Scheme of Fractional Ikeda-Based Memristor Map*

In the following, nonlinear controllers for achieving synchronization of the fractional Ikeda-based memristor map are presented. The synchronization process aims to minimize the error between the master map and the slave map, forcing it to converge toward zero. The commensurate fractional Ikeda-based memristor map, represented by Equation (19), is considered as the master map, whereas the slave Ikeda-based memristor map is defined as follows:

$$\begin{cases} {}^{c}\Delta_b^{\beta} y_{1s}(v) = 1 + \rho(y_{1s}(\varrho)\cos\psi_1(\varrho) - y_{2s}(\varrho)\sin\psi_1(\varrho)) + \mu(q_s^2(\varrho) - 1)y_{2s}(\varrho) - y_{1s}(\varrho) + U_1(\varrho), \\ {}^{c}\Delta_b^{\beta} y_{2s}(v) = \rho(y_{1s}(\varrho)\sin\psi_1(\varrho) + y_{2s}(\varrho)\cos\psi_1(\varrho)) - y_{2s}(\varrho) + U_2(\varrho), \\ {}^{c}\Delta_b^{\beta} q_s(v) = y_{2s}(\varrho) + U_3(\varrho). \end{cases} \tag{32}$$

$U_1$, $U_2$, and $U_3$ represent the synchronization controllers and:

$$\psi_1(\varrho) = 0.4 - \frac{0.6}{1 + y_{1s}^2(\varrho) + y_{2s}^2(\varrho)}$$

The fractional error map is defined as follows:

$$\begin{cases} {}^{C}\Delta_b^{\beta} e_1(v) = \rho(y_{1s}(\varrho)\cos\psi_1(\varrho) - y_{2s}(\varrho)\sin\psi_1(\varrho)) + \mu(q_s^2(\varrho) - 1)y_{2s}(\varrho) + U_1(\varrho) \\ \qquad - \rho(y_1(\varrho)\cos\psi(\varrho) - y_2(\varrho)\sin\psi(\varrho)) - \mu(q^2(\varrho) - 1)y_2(\varrho) - e_1(\varrho), \\ {}^{C}\Delta_b^{\beta} e_2(v) = \rho(y_{1s}(\varrho)\sin\psi_1(\varrho) + y_{2s}(\varrho)\cos\psi_1(\varrho)) + U_2(\varrho) - \rho\big(y_1(\varrho)\sin\psi(\varrho) \\ \qquad + y_2(\varrho)\cos\psi(\varrho)\big) - e_2(\varrho), \\ {}^{C}\Delta_b^{\beta} e_3(v) = e_2(\varrho) + U_3(\varrho) \end{cases} \tag{33}$$

The control rule proposed for establishing this synchronization scheme is outlined in the theorem presented below.

**Theorem 4.** *Subject to:*

$$\begin{cases} U_1(\varrho) = -\rho\Big(y_{1s}(\varrho)\cos\psi_1(\varrho) - y_1(\varrho)\cos\psi(\varrho) + y_2(\varrho)\sin\psi(\varrho) - y_{2s}(\varrho)\sin\psi_1(\varrho)\Big) \\ \qquad -\mu\Big(q_s^2(\varrho)y_{2s}(\varrho) - q^2(\varrho)y_2(\varrho)\Big), \\ U_2(\varrho) = -\rho\Big(y_{1s}(\varrho)\sin\psi_1(\varrho) - y_1(\varrho)\sin\psi(\varrho) + y_2(\varrho)\cos\psi(\varrho) - y_{2s}(\varrho)\cos\psi_1(\varrho)\Big) - \alpha_2 e_2(\varrho), \\ U_3(\varrho) = -e_2(\varrho) - \alpha_3 e_3(\varrho) \end{cases} \tag{34}$$

*where $-1 < \alpha_2 < 2^{\beta} - 1$ and $0 < \alpha_3 < 2^{\beta}$. Then, the master Ikeda-based memristor map (19) and slave Ikeda-based memristor map (32) are synchronized.*

**Proof.** Substituting the control law (34) into the fractional error map (33), we obtain:

$${}^{C}\Delta_d^{\beta}(e_1(v), e_2(v), e_3(v))^T = B \times (e_1(\varrho), e_2(\varrho), e_3(\varrho))^T, \tag{35}$$

where:

$$B = \begin{pmatrix} -(1+\mu) & 0 & 0 \\ 0 & -(1+\alpha_2) & 0 \\ 0 & 0 & -\alpha_3 \end{pmatrix}$$

The eigenvalues of the matrix $B$ are $\lambda_1 = -(1+\mu)$, $\lambda_2 = -(1+\alpha_2)$, and $\lambda_3 = -\alpha_3$. It is easy to see that for $\mu = 0.11$, $-1 < \alpha_2 < 2^{\beta} - 1$, and $0 < \alpha_3 < 2^{\beta}$, the eigenvalues satisfy the stability condition stated in Theorem 2, demonstrating that the zero solution of the fractional error map (33) is asymptotically stable, leading to the achieved synchronization of the master Ikeda-based memristor map (19) and the slave Ikeda-based memristor map (32). □

To confirm the validity of this result, numerical simulations are conducted using MATLAB. The specific parameter values chosen are $\beta = 0.9$, $\rho = 0.5$, $\mu = 0.11$, and the initial values $(e_1(0), e_2(0), e_3(0)) = (0.5, 0.2, -0.1)$. Figure 17 presents the time evolution of the states of the fractional error map (33). The figure clearly illustrates that the errors tend to zero, validating the effectiveness of the earlier discussed synchronization process.

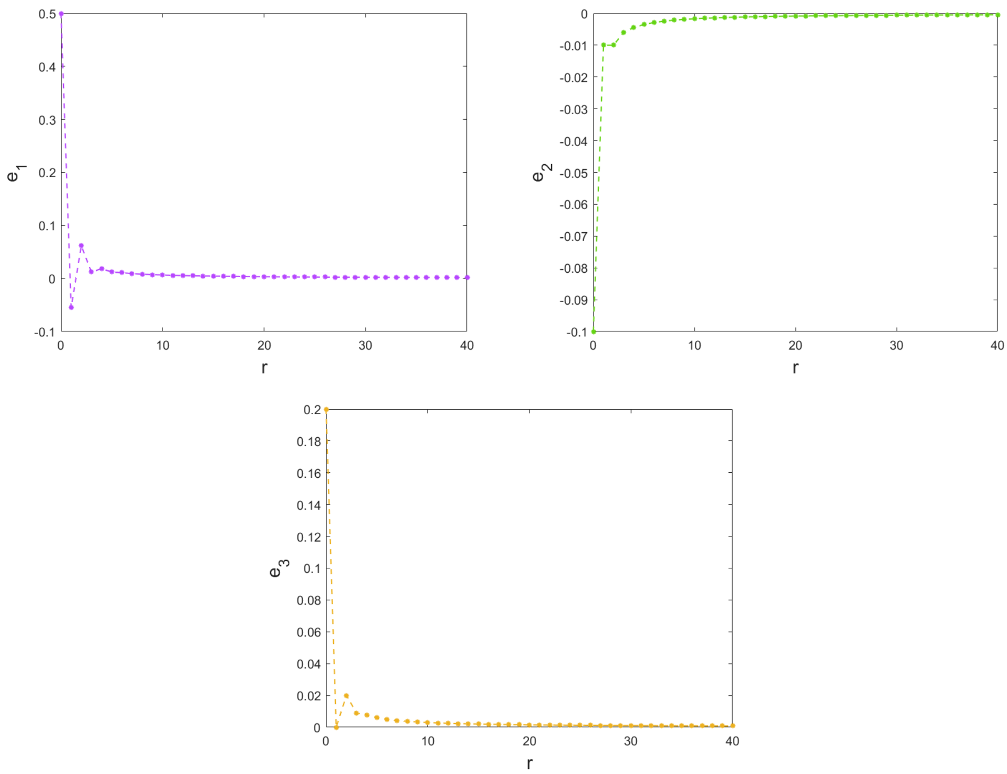


**Figure 17.** States of the fractional error map (33).

## 7. Conclusions

This article introduced a novel fractional Ikeda-based memristor map, investigating its behavior under commensurate and incommensurate fractional orders. The map's analysis exhibited diverse, dynamic characteristics, highlighting its rich dynamical nature. Through employing different methodologies analysis involving Lyapunov exponent calculations, bifurcations, and phase portraits, the distinct behaviors of the proposed fractional Ikeda-based memristor map were explored for both commensurate and incommensurate scenarios. Moreover, the complexity of the model was quantified using the sample entropy algorithm. The outcomes underscore the strong influence of the system parameter and fractional orders on the states of the fractional Ikeda-based memristor map. The values of these parameters hold pivotal significance in shaping the dynamics and behaviour of the system, and variations in their values lead to distinct trajectories and responses in the state space of the map. Ultimately, the paper proposes effective control laws that ensure the stabilization and synchronization of the introduced map by driving its states to asymptotically approach zero. The conducted numerical simulations provide a comprehensive understanding of the system's dynamics and highlight its interesting and diverse behaviors, which are of great importance in studying the implications of the fractional memristive maps.

**Author Contributions:** Conceptualization, O.A., A.A., N.A.-A., A.A.-H. and A.O.; Methodology, A.A., H.A.-T., M.A., G.M.G., M.S.A.S. and A.O.; Software, A.A., H.A.-T., M.A., M.S.A.S., N.A.-A. and A.O.; Validation, O.A., A.A., M.A., G.M.G., M.S.A.S. and A.O.; Formal analysis, A.A., N.A.-A. and A.O.; Investigation, O.A., A.A. and A.O.; Resources, O.A., A.A., H.A.-T., M.A., G.M.G., M.S.A.S., N.A.-A., A.A.-H. and A.O.; Data curation, O.A., A.A., H.A.-T., A.A.-H. and A.O.; Writing—original draft, A.A. and A.O.; Writing—review & editing, O.A., A.A., H.A.-T., M.A., G.M.G., M.S.A.S., N.A.-A., A.A.-H. and A.O.; Visualization, O.A., A.A., H.A.-T., M.A., G.M.G., M.S.A.S., N.A.-A. and A.A.-H.; Funding acquisition, O.A., A.A., H.A.-T., M.A., G.M.G., M.S.A.S., N.A.-A., A.A.-H. and A.O. All authors have read and agreed to the published version of the manuscript.

**Funding:** This research received no external funding.

**Data Availability Statement:** All data that support the findings of this study are included within the article.

**Conflicts of Interest:** The authors declare no conflict of interest.

## References

1. Pecora, L.M.; Carroll, T.L.; Johnson, G.A.; Mar, D.J.; Heagy, J.F. Fundamentals of synchronization in chaotic systems, concepts, and applications. *Chaos Interdiscip. J. Nonlinear Sci.* **1997**, *7*, 520–543. [CrossRef]
2. Yang, D., Liu, Z., Zhou, J. Chaos optimization algorithms based on chaotic maps with different probability distribution and search speed for global optimization. *Commun. Nonlinear Sci. Numer. Simul.* **2014**, *19*, 1229–1246. [CrossRef]
3. Chai, X., Zheng, X., Gan, Z., Han, D., Chen, Y. An image encryption algorithm based on chaotic system and compressive sensing. *Signal Process.* **2018**, *148*, 124–144. [CrossRef]
4. Xu, Q., Sun, K., Cao, C., Zhu, C. A fast image encryption algorithm based on compressive sensing and hyperchaotic map. *Opt. Lasers Eng.* **2019**, *121*, 203–214. [CrossRef]
5. Ditto, W., Munakata, T. Principles and applications of chaotic systems. *Commun. ACM* **1995**, *38*, 96–102. [CrossRef]
6. Vaidyanathan, S.; Volos, C. (Eds.). *Advances and Applications in Chaotic Systems*; Springer: Berlin, Germany, 2016; Volume 636, p. 445.
7. Zang, X.; Iqbal, S.; Zhu, Y.; Liu, X.; Zhao, J. Applications of chaotic dynamics in robotics. *Int. J. Adv. Robot. Syst.* **2016**, *13*, 60. [CrossRef]
8. Wang, X.; Su, Y.; Luo, C.; Nian, F.; Teng, L. Color image encryption algorithm based on hyperchaotic system and improved quantum revolving gate. *Multimed. Tools Appl.* **2022**, *81*, 13845–13865. [CrossRef]
9. Chua, L.O. Memristor-The missing circuit element. *IEEE Trans. Circuit. Theory* **1971**, *18*, 507–519. [CrossRef]
10. Strukov, D.B.; Snider, G.S.; Stewart, D.R.; Williams, R.S. The missing memristor found. *Nature* **2008** 453, 80–83. [CrossRef]
11. Ma, X.; Mou, J.; Liu, J.; Ma, C.; Yang, F.; Zhao, X. A novel simple chaotic circuit based on memristor—Memcapacitor. *Nonlinear Dyn.* **2020**, *100*, 2859–2876. [CrossRef]
12. Lin, T.C.; Huang, F.Y.; Du, Z.; Lin, Y.C. Synchronization of fuzzy modeling chaotic time delay memristor-based Chua's circuits with application to secure communication. *Int. J. Fuzzy Syst.* **2015**, *17*, 206–214. [CrossRef]
13. Sun, J.; Kang, K.; Sun, Y.; Hong, Q.; Wang, C. A multi-value 3D crossbar array nonvolatile memory based on pure memristors. *Eur. Phys. J. Spec. Top.* **2022**, *231*, 3119–3130. [CrossRef]
14. Bao, B.; Rong, K.; Li, H.; Li, K.; Hua, Z.; Zhang, X. Memristor-coupled logistic hyperchaotic map. *IEEE Trans. Circuits Syst. Regul. Pap.* **2021**, *68*, 2992–2996. [CrossRef]
15. Itoh, M.; Chua, L.O. Dynamics of memristor circuits. *Int. J. Bifurc. Chaos* **2014**, *24*, 1430015. [CrossRef]
16. Li, C.; Feng, B.; Li, S.; Kurths, J.; Chen, G. Dynamic analysis of digital chaotic maps via state-mapping networks. *IEEE Trans. Circuits Syst. Regul. Pap.* **2019**, *66*, 2322–2335. [CrossRef]
17. Rong, K.; Bao, H.; Li, H.; Hua, Z.; Bao, B. Memristive Hénon map with hidden Neimark–Sacker bifurcations. *Nonlinear Dyn.* **2022**, *108*, 4459–4470. [CrossRef]
18. Ramakrishnan, B.; Mehrabbeik, M.; Parastesh, F.; Rajagopal, K.; Jafari, S. A new memristive neuron map model and its network's dynamics under electrochemical coupling. *Electronics* **2022**, *11*, 153. [CrossRef]
19. Almatroud, O.A.; Pham, V.T. Building Fixed Point-Free Maps with Memristor. *Mathematics* **2023**, *11*, 1319. [CrossRef]
20. Chen, M.; Luo, X.; Suo, Y.; Xu, Q.; Wu, H. Hidden extreme multistability and synchronicity of memristor-coupled non-autonomous memristive Fitzhugh–Nagumo models. *Nonlinear Dyn.* **2023**, *111*, 7773–7788. [CrossRef]
21. Zhang, L.P.; Liu, Y.; Wei, Z.C.; Jiang, H.B.; Lyu, W.P.; Bi, Q.S. Extremely hidden multi-stability in a class of two-dimensional maps with a cosine memristor. *Chin. Phys. B* **2022**, *31*, 100503. [CrossRef]
22. Hilfer, R. (Ed.). *Applications of Fractional Calculus in Physics*; World Scientific: Singapore, 2000.
23. Atici, F.M.; Eloe, P. Discrete fractional calculus with the nabla operator. *Electron. J. Qual. Theory Differ. Equ. [Electron. Only]* **2009**, *2009*, 3. [CrossRef]
24. Anastassiou, G.A. Principles of delta fractional calculus on time scales and inequalities. *Math. Comput. Model.* **2010**, *52*, 556–566. [CrossRef]
25. Abdeljawad, T. On Riemann and Caputo fractional differences. *Comput. Math. Appl.* **2011**, *62*, 1602–1611. [CrossRef]
26. Wu, G.C.; Song, T.T.; Wang, S. Caputo—Hadamard fractional differential equations on time scales: Numerical scheme, asymptotic stability, and chaos. *Chaos Interdiscip. J. Nonlinear Sci.* **2022**, *32*, 093143. [CrossRef] [PubMed]
27. Majhi, S.; Perc, M.; Ghosh, D. Dynamics on higher-order networks: A review. *J. R. Soc. Interface* **2022**, *19*, 20220043. [CrossRef]
28. Wu, G.C.; Baleanu, D. Discrete fractional logistic map and its chaos. *Nonlinear Dyn.* **2014**, *75*, 283–287. [CrossRef]

29. Abbes, A.; Ouannas, A.; Shawagfeh, N.; Khennaoui, A.A. Incommensurate fractional discrete neural network: Chaos and complexity. *Eur. Phys. J. Plus* **2022**, *137*, 235. [CrossRef]
30. Shatnawi, M.T.; Abbes, A.; Ouannas, A.; Batiha, I.M. A new two-dimensional fractional discrete rational map: Chaos and complexity. *Phys. Scr.* **2022**, *98*, 015208. [CrossRef]
31. Hamadneh, T.; Abbes, A.; Falahah, I.A.; AL-Khassawneh, Y.A.; Heilat, A.S.; Al-Husban, A.; Ouannas, A. Complexity and Chaos Analysis for Two-Dimensional Discrete-Time Predator–Prey Leslie–Gower Model with Fractional Orders. *Axioms* **2023**, *12*, 561. [CrossRef]
32. Abbes, A.; Ouannas, A.; Shawagfeh, N. An incommensurate fractional discrete macroeconomic system: Bifurcation, chaos, and complexity. *Chin. Phys. B* **2023**, *32*, 030203. [CrossRef]
33. Khennaoui, A.A.; Ouannas, A.; Bendoukha, S.; Grassi, G.; Lozi, R.P.; Pham, V.T. On fractional–order discrete–time systems: Chaos, stabilization and synchronization. *Chaos Solitons Fractals* **2019**, *119*, 150–162. [CrossRef]
34. Saadeh, R.; Abbes, A.; Al-Husban, A.; Ouannas, A.; Grassi, G. The Fractional Discrete Predator–Prey Model: Chaos, Control and Synchronization. *Fractal Fract.* **2023**, *7*, 120. [CrossRef]
35. Ouannas, A.; Khennaoui, A.A.; Batiha, I.M.; Pham, V.T. Synchronization between fractional chaotic maps with different dimensions. In *Fractional-Order Design*; Academic Press: Cambridge, MA, USA, 2022; pp. 89–121.
36. Peng, Y.; He, S.; Sun, K. Chaos in the discrete memristor-based system with fractional-order difference. *Results Phys.* **2021**, *24*, 104106. [CrossRef]
37. Lu, Y.M.; Wang, C.H.; Deng, Q.L.; Xu, C. The dynamics of a memristor-based Rulkov neuron with the fractional-order difference. *Chin. Phys. B* **2022**, *31*, 060502. [CrossRef]
38. Ma, M.; Lu, Y.; Li, Z.; Sun, Y.; Wang, C. Multistability and phase synchronization of Rulkov neurons coupled with a locally active discrete memristor. *Fractal Fract.* **2023**, *7*, 82. [CrossRef]
39. Peng, Y.; Liu, J.; He, S.; Sun, K. Discrete fracmemristor-based chaotic map by Grunwald–Letnikov difference and its circuit implementation. *Chaos Solitons Fractals* **2023**, *171*, 113429. [CrossRef]
40. Shatnawi, M.T.; Abbes, A.; Ouannas, A.; Batiha, I.M. Hidden multistability of fractional discrete non-equilibrium point memristor based map. *Phys. Scr.* **2023**, *98*, 035213.
41. Lai, Q.; Lai, C.; Kuate, P.D.K.; Li, C.; He, S. Chaos in a simplest cyclic memristive neural network. *Int. J. Bifurc. Chaos* **2022**, *32*, 2250042. [CrossRef]
42. Ramadoss, J.; Natiq, H.; Nazarimehr, F.; He, S.; Rajagopal, K.; Jafari, S. A novel chaotic map with a shifting parameter and stair-like bifurcation diagram: Dynamical analysis and multistability. *Phys. Scr.* **2023**, *98*, 025212. [CrossRef]
43. Wang, J.; Gu, Y.; Rong, K.; Xu, Q.; Zhang, X. Memristor-based Lozi map with hidden hyperchaos. *Mathematics* **2022**, *10*, 3426. [CrossRef]
44. Bao, H., Hua, Z., Li, H., Chen, M., Bao, B. Discrete memristor hyperchaotic maps. *IEEE Trans. Circuits Syst. Regul. Pap.* **2021**, *68*, 4534–4544. [CrossRef]
45. Bao, B.C.; Li, H.; Wu, H.; Zhang, X.; Chen, M. Hyperchaos in a second-order discrete memristor-based map model. *Electron. Lett.* **2020**, *56*, 769–770. [CrossRef]
46. Kong, S.; Li, C.; He, S.; Çiçek, S.; Lai, Q. A memristive map with coexisting chaos and hyperchaos. *Chin. Phys. B* **2021**, *30*, 110502. [CrossRef]
47. Ikeda, K. Multiple-valued stationary state and its instability of the transmitted light by a ring cavity system. *Opt. Commun.* **1979**, *30*, 257–261. [CrossRef]
48. Ikeda, K.; Daido, H.; Akimoto, O. Optical turbulance: Chaotic behavior of transmitted light from a ring cavity. *Phys. Rev. Lett.* **1980**, *45*, 709–712 [CrossRef]
49. Laskaridis, L.; Volos, C.; Munoz-Pacheco, J.; Stouboulos, I. Study of the dynamical behavior of an Ikeda-based map with a discrete memristor. *Integration* **2023**, *89*, 168–177. [CrossRef]
50. Richman, J.S.; Moorman, J.R. Physiological time-series analysis using approximate entropy and sample entropy. *Am. J.-Physiol.-Heart Circ. Physiol.* **2000**, *278*, H2039–H2049. [CrossRef]
51. Li, Y.; Wang, X.; Liu, Z.; Liang, X.; Si, S. The entropy algorithm and its variants in the fault diagnosis of rotating machinery: A review. *IEEE Access* **2018**, *6*, 66723–66741. [CrossRef]
52. Čermák, J.; Győri, I.; Nechvátal, L. On explicit stability conditions for a linear fractional difference system. *Fract. Calc. Appl. Anal.* **2015**, *18*, 651–672. [CrossRef]